Injection-Induced Turbulence in Stagnation-Point Boundary Layers

Chul Park*
NASA Ames Research Center, Moffett Field, California

A theory is developed for the stagnation-point boundary layer with injection under the hypothesis that turbulence is produced at the wall by injection. From the existing experimental heat-transfer-rate data obtained in wind tunnels, the wall mixing length is deduced to be a product of a time constant and an injection velocity. The theory reproduces the observed increase in heat-transfer rates at high injection rates. For graphite and carbon-carbon composite, the time constant is determined to be 2×10^{-4} s from the existing ablation data taken in an arc-jet tunnel and a ballistic range.

Nomenclature

B_0 = blowing parameter referred to zero injection
C = $\rho(\mu+\epsilon)/(\rho_e\mu_e)$
C_d = turbulence dissipation coefficient, Eq. (11)
C_μ = eddy-viscosity coefficient, Eq. (3)
d = mixing length
d_m = limiting mixing length
e = turbulence energy
f = dimensionless stream function
f_w = dimensionless injection rate, Eq. (8)
G = turbulence dissipation parameter, Eqs. (10-12)
g = dimensionless enthalpy, Eq. (13)
H = enthalpy
h = dimensionless turbulence energy
K = correlation between momentum and mixing length, Eqs. (1) and (2)
m,n = exponents characterizing turbulence, Eq. (18)
Pr = Prandtl number (both laminar and turbulent)
q = heat-transfer rate
Re = Reynolds number based on freestream conditions and nose radius
Sc = Schmidt number (both laminar and turbulent)
T = temperature
t = time
u,v = velocity components tangential and normal to wall, respectively
x,y = distances tangential and normal to wall, respectively
α = species mass fraction
ϵ = turbulent eddy viscosity
η = dimensionless normal coordinate, Eq. (6)
μ = molecular viscosity
ρ = density
τ = eddy time constant (average time interval of fluctuation of injected flow)

Subscripts

e = edge of boundary layer
L = laminar
T = turbulent
w = wall
0 = zero injection
∞ = freestream condition

Received Jan. 13, 1983; revision received May 31, 1983. This paper is declared a work of the U. S. Government and therefore is in the public domain.

*Research Scientist, Entry Technology Branch. Member AIAA.

Introduction

THE role of turbulence in the boundary-layer flows at the stagnation point of a blunt body is one of the most interesting subjects in fluid mechanics. The classical boundary-layer theory does not allow for turbulence in the flow approaching the stagnation point. Existing experimental data show that the heat-transfer rates to the stagnation point of a cold body tested in a wind tunnel with no injection from the wall are generally higher than those predicted by the laminar theory.[1-3] The observed heat-transfer enhancement for the no-injection case has been attributed by Traci and Wilcox,[4] and more recently by Wassel and Denny,[5] to the interaction of boundary-layer flow with the turbulence in the test stream. According to the theory, the boundary layer amplifies the freestream turbulence, thereby modifying the average momentum and energy profiles in the boundary layer.

In atmospheric entry flights through a clear atmosphere or in ballistic range tests simulating such flights, turbulence is nonexistent in the freestream. Experimental data indicate that the boundary layer is indeed laminar at the stagnation point under these circumstances, provided there is little or no albation.[6,7] This is true even when the wall surface is not perfectly smooth; the effect of slight surface roughness is merely to induce an early boundary-layer transition to turbulence at a point downstream of the stagnation point.

Anomalous phenomena are found when the stagnation-point heat-transfer rates are sufficiently high to cause strong ablation. The results of the passive nose-tip technology (PANT) program indicate that the rates of ablation of graphite models tested in both a ballistic range and an arc-jet wind tunnel at very high heating rates are sometimes much higher than those predicted by the laminar theory.[8] The models that incurred a high ablation rate showed rough and irregular surface appearances. The ablation rates agreed with the calculations in which turbulence caused by surface roughness and spallation are accounted for and in which the convective shielding owing to injection is ignored.[8] It remains to be explained, however, why the convective-shielding effect should be neglected. According to Ref. 9, surface roughness in the stagnation region merely causes the boundary layer to slip, and forms a laminar flow at the roughness edge in the presence of a large injection. In order to justify the interpretation of Ref. 8, one must show how turbulence is produced from the injecting surfaces.

Valuable clues to the nature of the boundary layer with finite-mass injection have been obtained recently. In tests conducted in a wind tunnel, Demetriades et al.[10] measured velocity distributions in the boundary layer a short distance away from the stagnation point to show that the boundary-layer flow, which is otherwise laminar, becomes turbulent as

mass-injection rate increases. Shadowgraphs taken by Kaattari[11] show that even if the test-gas stream is nearly free of turbulence, the boundary-layer flow is strongly turbulent at large mass-injection rates. Feldhuhn[12] and Kaattari[13] independently measured heat-transfer rates at the stagnation point at varying rates of mass injection. At low injection rates their results show a decrease in heat-transfer rates in accordance with the convective shielding predicted by the laminar theory.[14] This convective-shielding phenomenon becomes ineffective beyond a certain finite injection rate: the heat-transfer rates remain nearly constant for injection rates greater than a certain value.

It is evident from these results that boundary-layer flows become turbulent at the stagnation point when the mass-injection rate is high. At present, however, there is no theory that satisfactorily explains this phenomenon. The purpose of this work is to develop such a theory. This is accomplished by 1) hypothesizing that turbulence is induced at the wall by the mass injection, and 2) adopting the formulation of Wassel and Denny[5] for the calculation of the distribution of turbulence energy in the boundary layer. By comparing the resulting theoretical heat-transfer rates with the wind tunnel test data,[12,13] it is deduced that the mixing length in the turbulence produced by the mass injection is proportional to the injection rate. The constant of proportionality is determined for the wind tunnel[8,12,13] and ballistic range,[8,15] test conditions using the existing data.

Nature of Injection-Induced Turbulence

There are several possible mechanisms by which turbulence could be initiated in a flow produced by the injection from a wall; four of these are illustrated schematically in Figs. 1a-d. Figure 1a shows the case in which the mass is injected from an array of relatively large, uniformly sized and spaced holes drilled through the wall. In this case, the jet flows induce vortices in the directions shown by the curved arrows. If the Reynolds numbers characterizing the jet flows are sufficiently large, these vortices survive the viscous dissipation and become the source of turbulence in the boundary layer. Whether or not the boundary layer would support or suppress these possible sources of turbulence is dependent on the Reynolds number characterizing the boundary layer. The mixing length in the turbulence will be roughly of the order of the size of the vortices. In Fig. 1b, the holes are sufficiently small so that the local vortices are dissipated by the viscous forces. However, here the hole diameters are not uniform and the holes are placed at irregular intervals. The flows from the more closely spaced or large holes coalesce to form a large mean flow, as shown in the figure. The resulting flow is similar to that of Fig. 1a. Figure 1c illustrates the case in which such coalescence is caused by the irregularity in the direction of injection from the individual holes. In Fig. 1d, the injection occurs in the form of thermochemical sublimation at the wall surface and is, therefore, microscopically uniform. However, the surface is curved (i.e., rough) in this case, and this causes variation in the regionally averaged mass-flow rates. The sizes of the vortices, and, hence, the mixing lengths, will be roughly equal to the scales of the surface roughnesses in this case.

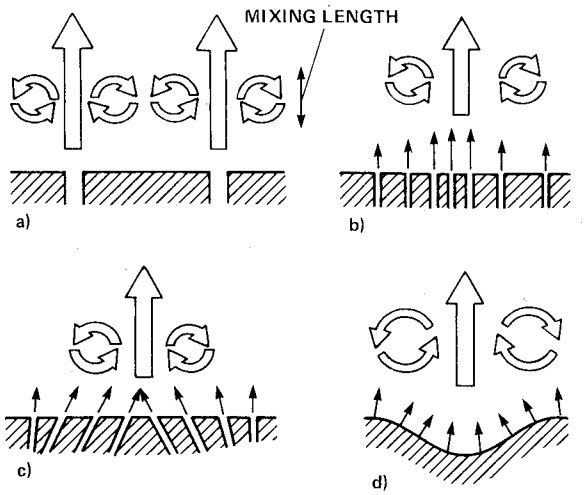

Fig. 1 Schematic of the injection mechanisms leading to turbulence. a) Large uniformly spaced and sized injection holes; b) small-diameter nonuniformly spaced holes; c) irregularly angled holes; d) thermochemical sublimation on curved wall.

According to the mixing-length theory of turbulence, eddy viscosity can be expressed as a time average of the product of the fluctuating component of the cross-flow momentum and a mixing length. The fluctuating component of the normal momentum is likely to be proportional to the injection flow rate in the present problem. Therefore, the eddy viscosity of the flow at the surface produced by the injection can be written for the present problem in the form

$$\epsilon_w = K\rho_w v_w d \tag{1}$$

where ρ, v, and d are the time-averaged density, normal velocity, and mixing length, respectively, and the coefficient K is an empirical constant. The subscript w denotes wall values. To reduce the number of unknown parameters to a minimum, the constant is assumed (arbitrarily) in the present work to be

$$K = 0.4 \tag{2}$$

which is the value of the von Kármán constant for the mixing length for the turbulent boundary layer on a flat plate in equilibrium. It is possible also to express the eddy viscosity in terms of turbulence energy in the form

$$\epsilon = C_\mu \rho e^{1/2} d \tag{3}$$

where C_μ is the constant of proportionality of the eddy viscosity, and e is the kinetic energy of the turbulence. Following Wassel and Catton,[17] the coefficient C_μ is taken to be

$$C_\mu = 0.1455 \tag{4}$$

Equations (1-4) provide the means for determining e_w from ρ_w and v_w.

The mixing length d must be determined experimentally. Figure 2 is a reproduction of the shadowgraphs taken by Kaattari,[11] which shows the flowfield induced by the injection of helium and Freon in the stagnation region against an air stream. From the photograph, the eddy sizes are seen to be essentially unchanged throughout the blowing layer. Hence, the assumption is made here that

$$\frac{\mathrm{d}(d)}{\mathrm{d}y} = 0 \tag{5}$$

where y is the normal distance measured from the wall. The numerical value of d will be determined later by comparing the calculated heat- and mass-transfer rates with the experimental data.

Boundary-Layer Equations

In the stagnation region of a blunt body, the pressure is nearly constant and the velocity is nearly zero. In most practical problems, the flow in this region is laminar, and, hence, a similarity solution is possible. When mass injection is present, as discussed above, it can affect the surface viscosity by creating a region of local turbulence. Wassel and Denny[5] have shown that a similarity-type solution is still possible by means of an eddy-viscosity coefficient when the effect of the

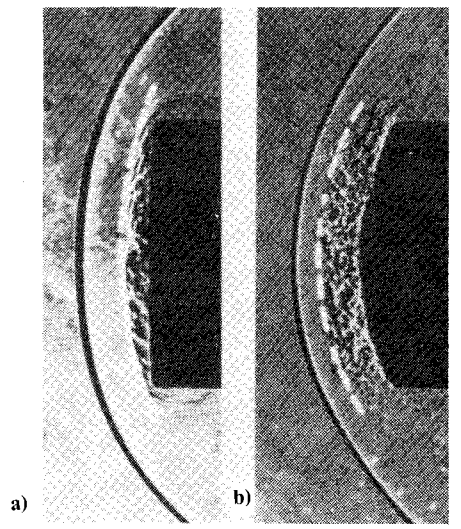

Fig. 2 Shadowgraphs of flows around models of overall diameter of 3.81 cm in Mach 5 airstream with injection, stagnation pressure of 0.1 atm. a) Helium injection, $\dot{m}/(\rho_\infty v_\infty)=0.067$. b) Freon injection, $\dot{m}/(\rho_\infty v_\infty)=0.63$. (Reproduced from Ref. 11.)

local turbulence is included. In the stagnation region there are only two actions that affect the turbulence produced by the injected mass: diffusion and viscous dissipation. The turbulence produced at the wall diffuses toward the edge of the boundary layer; while so doing, it decays because of the viscous dissipation. By definition, the intensity of the turbulence must vanish at the edge of the boundary layer. Wassel and Denny[5] solved an opposite, but very similar, case in which turbulence was introduced at the boundary-layer edge and decayed toward the wall. The equations governing the present problem are identical to those used by Wassel and Denny.

Following Wassel and Denny, the present work adopts the nondimensional normal coordinate η defined as

$$\eta=\left[2\rho_e\frac{(\mathrm{d}u_e/\mathrm{d}x)_0}{\mu_e}\right]^{-1}\int_0^y\frac{\rho}{\rho_e}\mathrm{d}y \tag{6}$$

Conservation of time-averaged mass and momentum is governed by the equation

$$(Cf'')'+ff''+\tfrac{1}{2}(\rho_e/\rho-(f')^2)=0 \tag{7}$$

where

$$C=\rho(\mu+\epsilon)/(\rho_e\mu_e)$$

The boundary conditions for Eq. (7) are:

$$\text{at } \eta=0 \quad f=-f_w=-\rho_w v_w\,[2\rho_e\mu_e(\mathrm{d}u_e/\mathrm{d}x)_0]^{-\frac{1}{2}}$$
$$\text{and } f'=0 \tag{8}$$

and $f'=1$ at $\eta=\infty$.

The turbulence energy is expressed in terms of the normalized variable h defined as

$$h=e/e_w=[(\rho_w/\rho)(\epsilon/\epsilon_w)]^2 \tag{9}$$

The quantity h satisfies the equation[5]

$$(Sc^{-1}Ch')'+fh'-Gh^{3/2}=0 \tag{10}$$

where Sc is the effective Schmidt number and G is defined by

$$G=\tfrac{1}{2}C_d(\mathrm{d}u_e/\mathrm{d}x)_0^{-1}e_w^{\frac{1}{2}}d^{-1} \tag{11}$$

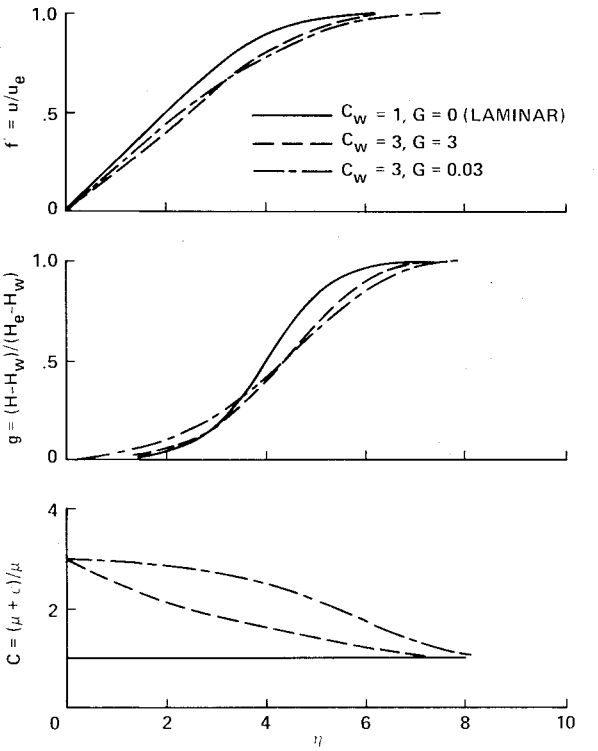

Fig. 3 Typical boundary-layer profiles with injection-induced turbulence; incompressible flow with $f_w=-2$.

The parameter C_d is the dissipation coefficient which is taken here to be[17]

$$C_d=0.42$$

The three terms in Eq. (10) represent diffusion, convection, and dissipation of turbulence energy, respectively. Boundary conditions for Eq. (10) are

$$h=1 \quad \text{at} \quad \eta=0$$
$$=0 \quad \text{at} \quad \eta=\infty$$

Using Eqs. (1-4) and (8), and the approximation $\rho_e\mu_e/\rho_w\mu_w=1$ (for the calculation of G only), the parameter G becomes

$$G=2.89(Kf_w)^2(\mu_w/\epsilon_w) \tag{12}$$

The equation of energy transfer is simplified in the present work by adopting the frozen-flow approximation, and by assuming the Lewis number (Pr/Sc) to be unity (for both molecular and turbulent properties). In terms of the normalized enthalpy,

$$g=(H-H_w)/(H_e-H_w) \tag{13}$$

the equation of energy conservation then becomes

$$(Pr^{-1}Cg')'+fg'=0 \tag{14}$$

where Pr is the Prandtl number. The boundary conditions for Eq. (14) are

$$g=0 \quad \text{at} \quad \eta=0$$
$$=1 \quad \text{at} \quad \eta=\infty$$

Mass transfer across the boundary layer is governed by the species-conservation equation. Denoting the mass fraction of

a species under consideration as α, the governing equation becomes, under the assumption of a frozen flow,

$$(Sc^{-1}C\alpha')' + f\alpha' = 0 \tag{15}$$

The boundary conditions of the species equation are, at $\eta = 0$,

$$\rho D(\partial\alpha/\partial y) + \rho v\alpha$$

$$= \text{rate of surface production of species } \alpha \tag{16}$$

At $\eta = \infty$, $\alpha = \alpha_e$. The present work assumes $Pr = Sc = 0.667$. Solution of the above system of equations yields the heat- and mass-transfer rates at the wall. In the following sections the results of such solutions are presented.

General Features of the Solutions

For the simplest case of incompressible flow, the boundary-layer solutions are dependent only on $C_w = \rho_w(\mu_w + \epsilon_w)/(\rho_e\mu_e)$ and G. C_w is used here as a measure of the value of ϵ_w. In Fig. 3 two typical solutions are obtained for arbitrarily chosen sets of C_w and G values and compared with the laminar solutions. As seen in the figure, both the velocity and energy profiles become flatter, resulting in a thicker boundary layer. The wall slopes of these profiles are, therefore, slightly smaller than the slopes in laminar flow. The eddy viscosities decrease monotonically from the wall value to zero at the edge of the boundary layer. The decrease is more rapid for a larger G; G represents the magnitude of viscous dissipation, and so a larger value of G induces a more rapid dissipation of turbulence energy.

In Fig. 4, the calculated wall-shear parameter $(Cf'')_w$, heat-transfer parameter $(Cg')_w$, and mass-transfer parameter $(C\alpha')_w/(\alpha_e - \alpha_w)$ are presented for the incompressible case for various values of ϵ_w/μ_w as a function of f_w. For any given value of f_w, all three parameters increase monotonically as ϵ_w/μ_w increases. This occurs despite the fact that the wall slopes of velocity (f_w''), energy (g_w'), and species profiles (α_w') are smaller; the increase in C_w is dominant in $(Cf'')_w$, etc. The convective-shielding effect is compromised seriously as a result. Over a fairly broad range (of small f_w, large ϵ_w/μ_w), the calculated heat-transfer parameter is larger than the laminar value at zero injection; i.e., a "negative" convective shielding occurs.

In the range of weak turbulence,

$$C_w < 6 \quad \text{and} \quad -f_w < 2$$

the ratio of turbulent to laminar heat- and mass-transfer-rate parameters can be approximated for the incompressible case by

$$\frac{(Cg')_{wT}}{(Cg')_{wL}} = \frac{(C\alpha')_{wT}}{(C\alpha')_{wL}} = C_w^{0.415}\exp[0.667(C_w)^{1/2}|f_w|] \tag{17}$$

Mixing Lengths for Injection through Porous Metal Walls

According to the present theoretical model, the mixing length is a constant determined only by the method of injection and the flow environments. The mixing length is determined first for the wind tunnel test conditions of Feldhuhn[12] and Kaattari.[13] In the work of Feldhuhn, air was passed through the model wall, which was made of porous beryllium-copper; Kaattari used sintered stainless steel. Their data, reproduced in Fig. 5, consist of the convective heat-transfer rates measured at the stagnation point as a function of the blowing parameter B_0. This parameter, which refers to the mass-transfer rate at zero blowing,[14] is related to f_w in these cases by $B_0 \cong -1.85f_w$. The two porous wall materials used by the two investigators are significantly different in their porosity and surface roughness; hence, the mixing length

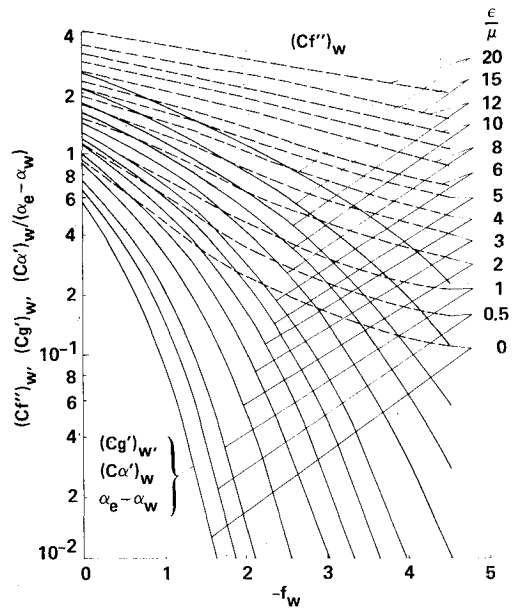

Fig. 4 Wall-shear parameter $(Cf'')_w$, heat-transfer-rate parameter $(Cg')_w$, and mass-transfer parameter $(C\alpha')_w/(\alpha_e - \alpha_w)$ in an incompressible flow with injection-induced turbulence.

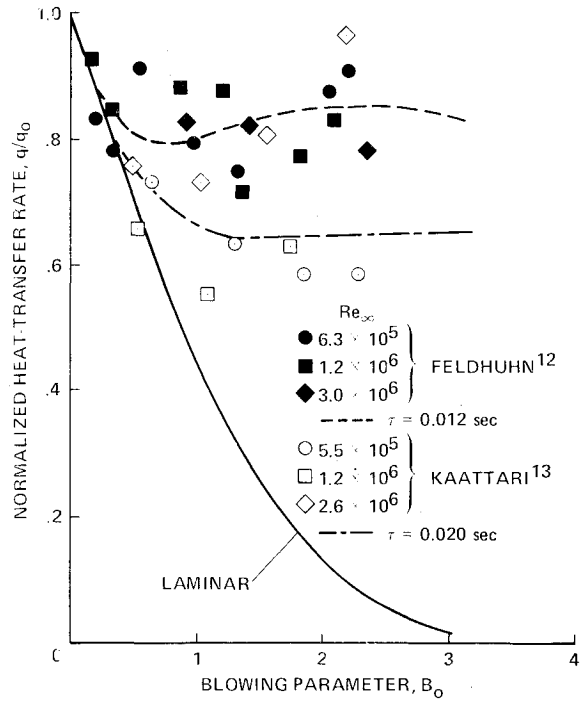

Fig. 5 Comparison of the present theory and experiments of Feldhuhn[12] (beryllium) and Kaattari[13] (stainless steel).

is deduced separately for the two cases. The temperature varied across the boundary layer by a ratio of about 1.4 for the tests of Feldhuhn, and by 2.6 for those of Kaattari. The ratio ρ_e/ρ in Eq. (7) is calculated for these cases, using the solutions of the energy equation (14) and the ideal gas law. The viscosity variation within the boundary layer is approximated by $\mu \propto T^{0.7}$.

To determine the mixing length, first assume its functional form with respect to environmental parameters. In the region of low injection rates, mixing length d is dictated by the balance, through a yet unknown mechanism, between the inertial and viscous forces. Hence, the Reynolds number of

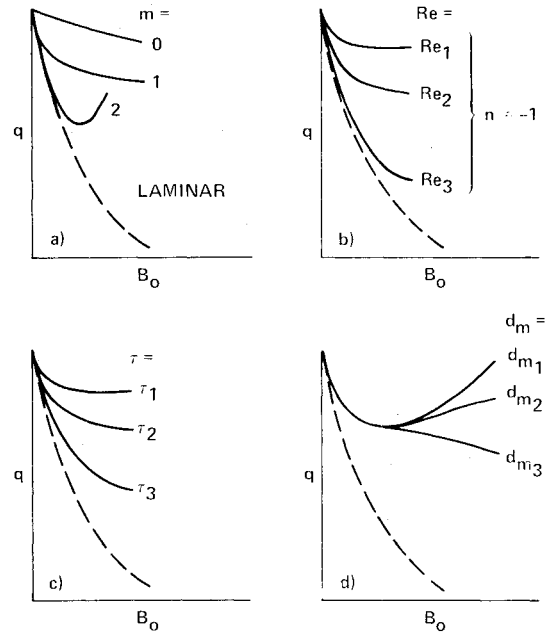

Fig. 6 Effect of the parameters m, n, τ, and d_m on calculated turbulent heat-transfer rate q at various f_w; a) m, b) n, c) τ, d) d_m.

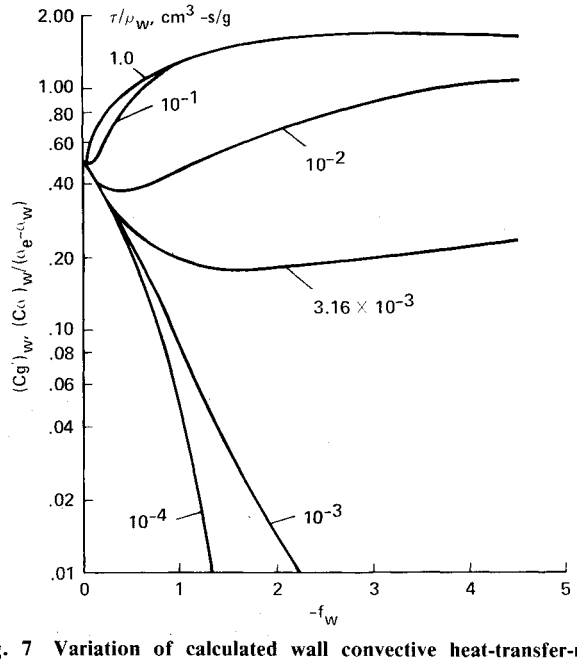

Fig. 7 Variation of calculated wall convective heat-transfer-rate parameter $(Cg')_w$ and mass-transfer-rate parameter $(C\alpha')_w/(\alpha_e - \alpha_w)$ with f_w for various τ/ρ_w; $\mu_w = 1.39 \times 10^{-3}$ poise, $T_e/T_w = 3.11$, $\dot{m} = -1.49 f_w$ g cm^2 s^{-1}, $(dy/d\eta) = 1.32 \times 10^{-3}$ cm.

the vortices induced by the wall injection can be written in general as a function of some unknown powers of density and injection velocity; i.e.,

$$\frac{\text{inertial force}}{\text{viscous force}} = \frac{\rho_w v_w d}{\mu_w} = c\rho_w^a v_w^b$$

where c is a function only of the surface topography. This relationship can be written also as

$$d = \tau \dot{m}^m \rho_w^n$$

where τ is a function of the wall topography and viscosity only. Since the mixing length cannot grow indefinitely at large $\dot{m}^m$ or ρ_w^n, it must have a limiting value. A simple functional form that satisfies these constraints is

$$d = d_m[1 - \exp(-\tau \dot{m}^m \rho_w^n / d_m)] \tag{18}$$

where d_m is the limiting value.

The boundary-layer calculations described earlier are carried out for the two wind tunnel test environments with m, n, τ, and d_m as arbitrary parameters. Figures 6a-d show the effects of these parameters on the calculated stagnation-point heat-transfer rate (q) values. The parameters are determined through the following steps:

1) The parameter m describes the behavior of the q vs B_0 curve at small B_0 (see Fig. 6a). The wind tunnel test data (Fig. 5) agree best with $m = 1$.

2) If n is not equal to -1, the calculated q values are dependent on the flow Reynolds numbers Re at small B_0 (Fig. 6b). The wind tunnel data show no discernible dependence of q on Re. Hence $n = -1$.

3) The quantity τ determines the numerical value of q at small B_0 when $m = 1$ and $n = -1$ (Fig. 6c). The matching τ values are found by comparing the calculated q values with the experimental data.

4) The limiting mixing length d_m determines q at high B_0 (Fig. 6d). The calculated q values become dependent on the flow Reynolds number, unless d_m is proportional to the boundary-layer thickness. The boundary-layer edge corresponds to a value of η of about 5 (see Fig. 3). Consequently, the boundary-layer thickness

$$\int_0^{\eta_e} \frac{dy}{d\eta} d\eta$$

becomes, for the present nearly incompressible case, nearly equal to $5(dy/d\eta)_w$. Hence, d_m is deduced to be a constant multiple of $(dy/d\eta)_w$.

With $m = 1$ and $n = -1$, Eq. (18) becomes

$$d = d_m[1 - \exp(-\tau v_w / d_m)] \tag{19}$$

At low injection rates, Eq. (19) becomes

$$d = \tau v_w \tag{20}$$

That is, the mixing length is a product of a time constant and injection velocity. The time constant can be interpreted as the average time interval of the fluctuation of the injected flow that modulates it. Since viscosity, and hence τ, is a weak function of molecular mass, Eq. (20) correctly reproduces the fact that an injectant gas of heavier molecular weight produces smaller eddies[11] (see Fig. 2). Good agreement between the theory and the experiment is found for the two wind tunnel test conditions, with the d_m and τ values given by

$$d_m = 35(dy/d\eta)_w \tag{21}$$

$$\tau = 0.012 \text{ s (beryllium-copper}^{12}\text{)} \tag{22}$$

$$\tau = 0.020 \text{ s (sintered stainless steel}^{13}\text{)} \tag{23}$$

The theoretical heat-transfer-rate values calculated with these values are shown in Fig. 5 and are compared with the experimental data. The difference between the time constant τ for the two materials is understandable, considering the differences in their porosity and surface roughness. The limiting mixing lengths predicted by Eq. (21) roughly match the sizes of the largest eddies seen in the shadowgraphs of Kaattari[11] (see Fig. 2).

In Fig. 7, the convective heat-transfer-rate parameter $(Cg')_w$ and the mass-transfer-rate parameter $(C\alpha')_w/(\alpha_e - \alpha_w)$ calculated for a typical condition attainable in a ballistic range[8] are shown for various assumed values of the ratio

τ/ρ_w. For the case shown, the calculated quantity is a sensitive function of this ratio when the ratio is in the range 0.001–0.1. For ratio values greater than 0.1, the transfer-rate parameters asymptotically approach a limiting curve. The limiting curve reaches a value that is 3.5 times the no-blowing value for the case shown. The parameters are orders of magnitude greater than the laminar values at large f_w.

At large values of τ/ρ_w the slopes of the curves become positive. In this positive-slope range an increase in ablation rate causes an increase in heat- and mass-transfer rates. If these increases are too great to be offset by the cooling effect of ablation, a further increase in heat- and mass-transfer rates will occur, leading to an instability. This instability causes numerical difficulty in the time integration of the ablation process: a small truncation error is amplified into a large error.

Mixing Length for Ablating Graphite and Carbon-Carbon

In Ref. 8 (PANT tests), ablation rates of ATJS graphite are measured in an airstream for a model (1.27 cm radius) in high-heating environments using an arc-jet wind tunnel and a ballistic range. In the ballistic range tests, the models are launched at a speed of about 5.4 km/s into ambient air at a pressure of 0.1–0.8 atm. The arc-jet tests produced conditions similar to those in the ballistic range. The ablation data obtained in these tests are reproduced in Fig. 8.

The turbulent boundary-layer calculations described earlier are repeated for the conditions of Ref. 8. The density ratio ρ_e/ρ in Eq. (7) is assumed to vary as in a perfect gas, dictated only by the temperature ratio across the boundary layer. The thermochemistry of air is simplified by neglecting the formation of atomic nitrogen and nitric oxide, and by assuming oxygen to be fully dissociated. Thus air is assumed to consist only of molecular nitrogen (N_2) and atomic oxygen (O). At the wall, atomic oxygen reacts with the surface to form carbon monoxide (CO), via

$$O + C(c) \rightarrow CO + 30{,}000 \text{ J/(g of graphite)}$$

The species to be considered in this formulation, therefore, are N_2, O, CO, and the product of subliminaton of graphite. For N_2, the right-hand side of Eq. (16) is zero. For O and CO, the right-hand side of Eq. (16) expresses the surface oxidation rate. The expression and the rate value for the process are taken from Ref. 18. For the ablation product, the right-hand side of Eq. (16) becomes a Knudsen-Langmuir equation.[19] The ablation rate is determined using the steady-state assumption and the heat-of-sublimation value of 31,000 J/g.

The validity of the simplified thermochemistry is verified by comparing the calculated results with the published equilibrium-flow solution for laminar flow. It is known that the frozen-flow method, such as the one used here, yields approximately the same results as the equilibrium-flow method.[14,20] The present method was found to give the ablation rates that deviate less than 5% from those given by the equilibrium-flow method in the range of interest.[21]

For the conditions of the PANT tests, the limiting mixing length d_m is deduced from the combination of Eq. (21) and the roughness of the model surfaces. For these tests, Eq. (21) gives a thickness smaller than the scale of the surface roughnesses, and, hence, does not express the full extent of mixing length. The data show that the surface roughness is more severe at higher pressures. At the highest pressures tested (i.e., 250 atm) the roughness scale is of the order of 0.1 cm. The limiting mixing length is assumed here, therefore, to be the larger between Eq. (21) and

$$d_m = 0.1(p/250)^{1/2} \text{ cm}$$

where the stagnation pressure p is in atm.

Figure 8 compares the results of the present calculation with the experimental data. As shown in the figure, almost all

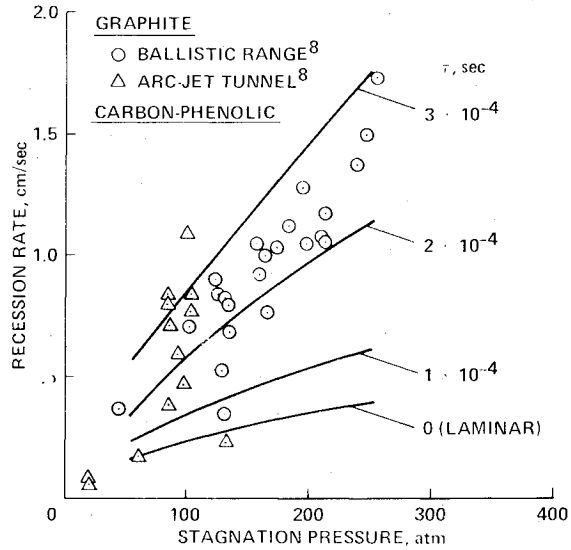

Fig. 8 Comparison of the measured and calculated recession rates for nose radius of 1.27 cm: ATJS graphite and carbon-phenolic in air.

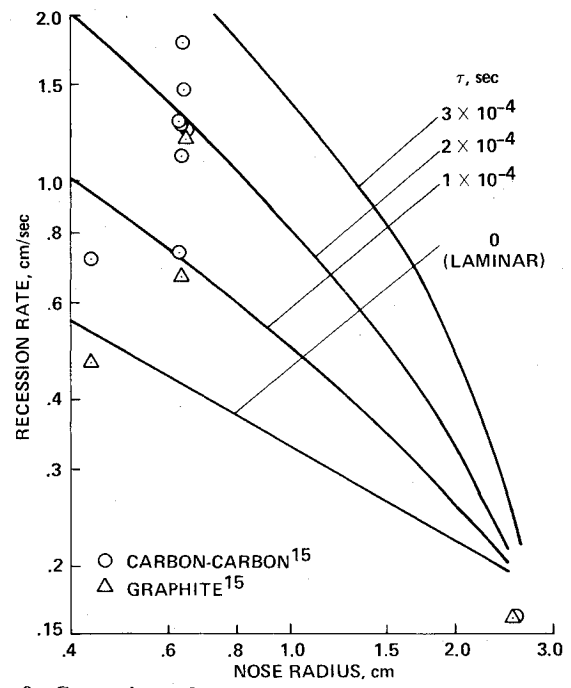

Fig. 9 Comparison of the measured and calculated recession rates for carbon-carbon and ATJS graphite models of varying nose radius; launched in a ballistic range at 450 Torr.

experimental data fall between the laminar values ($\tau = 0$) and the turbulent values based on $\tau = 3 \times 10^{-4}$ s. Such a wide scatter can be attributed to the lack of reproducibility of surface roughness. The two data points plotted at a pressure of about 20 atm (Fig. 8) lie slightly below the laminar theoretical value. This may be because of the possibility that steady-state conditions had not been achieved at those conditions. At such low pressures, the heat-transfer rate is too low to produce a steady-state ablation throughout the flight duration. The residual heat in the model at the end of the flight constitutes a significant portion of the total energy transmitted into the wall in this case. Most of the data points lie between the curves corresponding to $\tau = 2 \times 10^{-4}$ and 3×10^{-4} s. Assuming a spallation contribution to the recession rate,[22] a reasonable value of the time constant can be taken to be

$$\tau = 2 \times 10^{-4} \text{ s (graphite)} \qquad (24)$$

The unclassified portion of Ref. 15 presents the recession data for models of varying nose radii made of carbon-carbon composite and ATJS graphite tested in the same ballistic range. For most of the data the range pressure was 450 Torr. The present theory is applied to these test conditions for models having nose radii greater than 0.4 cm. For the smaller models, the present theory is inappropriate because the roughness dimensions approach the dimensions of the nose radius. In Fig. 9, the theoretical and experimental results are compared. As in Fig. 8, most experimental data are within the limits defined by the $\tau=0$ and $\tau=3\times10^{-4}$ s. Thus, carbon-carbon composite seems to behave approximately the same way as graphite in producing turbulence.

Figure 9 shows that the theoretical turbulent recession rates converge to the laminar value for large nose radii. At large nose radii, the turbulent solutions predict recession rates of less than 0.25 cm/s. At such low recession rates the eddy viscosity of the turbulence produced by injection is fairly small.

Discussion

The theory expounded here successfully explains 1) the two available sets of heat-transfer data with wall injection obtained in wind tunnels and 2) the two sets of ablation data for graphite and carbon-carbon composite obtained in an arc-jet wind tunnel and in a ballistic range. For the two carbonaceous materials, the time constant τ is found to be about 2×10^{-4} s. Recently, ablation tests were conducted for carbon-phenolic and the results obtained conform with the theory presented here—a time constant τ value of 2×10^{-4} s. The details of this more recent work will be the subject of a separate paper. Other existing data are found to be inappropriate for comparison with the present theory. For instance, the velocity-profile measurement of Demetriades et al.[10] was made at a point sufficiently far away from the stagnation point for the boundary-layer shear to affect turbulence. The arc-jet ablation measurements of graphite[23] and of carbon-phenolic[24] were made at injection rates too low for turbulence to be significant, for example, at $\epsilon_w/\mu_w \leq 0.1$. The ballistic-range ablation tests of carbon-phenolic and other materials in Ref. 25 were made with models of very small nose radii. These nose radii were of the same order as the surface roughness, and, consequently, the present analysis is inapplicable. The ablation tests with carbon-phenolic and carbon-carbon composite models described in Ref. 26 were made in a radiation-dominated regime where turbulence had little effect on ablation rates.

Conclusions

The results of four existing sets of experimental heat-transfer and ablation-rate data agree with a proposed theory based on the hypothesis that turbulence is initiated by the wall injection, and that its mixing length is proportional to the injection velocity. Eddy viscosity at the wall is given by $\epsilon_w = 0.4\dot{m}d_m\{1-\exp[-\tau\dot{m}/(\rho_w d_m)]\}$ where the time constant τ is 2×10^{-4} s for graphite, carbon-carbon, and carbon-phenolic. Heat- and mass-transfer rates are increased drastically by the injection-induced turbulence. For a weak turbulence in an incompressible flow, the transfer rates are increased, approximately, by the ratio $C_w^{0.42}\exp[0.667(C_w)^{1/2}|f_w|]$ where $C=\rho(\mu+\epsilon)/(\rho_e\mu_e)$.

Acknowledgments

The author wishes to express his sincere thanks to Mr. M. W. Rubesin and his colleagues in the Experimental Fluid Dynamics Branch, Ames Research Center, for their valuable suggestions and encouragement.

References

[1] Kestin, J., "The Effect of Free-Stream Turbulence on Heat Transfer Rates," *Advances in Heat Transfer*, Vol. 3, Academic Press, New York, 1966, pp. 1-32.

[2] Galloway, T. R., "Enhancement of Stagnation Flow Heat and Mass Transfer through Interaction of Freestream Turbulence," *AIChE Journal*, Vol. 19, No. 3, May 1973, pp. 608-617.

[3] Gostowski, V. J. and Costello, F. A., "The Effects of Freestream Turbulence on the Heat Transfer from the Stagnation Point of a Sphere," *International Journal of Heat and Mass Transfer*, Vol. 13, No. 8, May 1970, pp. 1382-1386.

[4] Traci, R. M. and Wilcox, D. C., "Freestream Turbulence Effects on Stagnation-Point Heat Transfer," *AIAA Journal*, Vol. 13, July 1975, pp. 890-896.

[5] Wassel, A. T. and Denny, V. E., "Heat Transfer to Axisymmetric Bodies in Super- and Hypersonic Turbulent Streams," *Journal of Spacecraft and Rockets*, Vol. 14, April 1977, pp. 212-218.

[6] Reda, D. C., "Comparative Transition Performance of Several Nosetip Materials as Defined by Ballistic-Range Testing," *Instrument Society of America Transactions*, Vol. 19, No. 1, Jan.-March 1980, pp. 83-98.

[7] Reda, D. C., "Correlation of Nosetip Boundary-Layer Transition Data Measured in Ballistic-Range Experiments," *AIAA Journal*, Vol. 19, March 1981, pp. 329-339.

[8] Wool, M. R., "Final Summary Report Passive Nosetip Technology (PANT) Program," SAMSO/RSSE, Los Angeles, Calif., SAMSO-TR-75-250, June 1975.

[9] Libby, P. A., "Interaction of a Rough Subliming Surface and a Laminar Boundary Layer," *AIAA Journal*, Vol. 16, Feb. 1978, pp. 130-136.

[10] Demetriades, A., Laderman, A. J., Von Seggern, L., and Hopkins, A. T., "Effects of Mass Addition on the Boundary Layer of a Hemisphere at Mach 6," *Journal of Spacecraft and Rockets*, Vol. 13, Aug. 1976, pp. 508-509.

[11] Kaattari, G. E., "Effects of Simulated Ablation Gas Injection on Shock Layer of Blunt Bodies at Mach 3 and 5," NASA TN D-2954, 1965.

[12] Feldhuhn, R. H., "Heat Transfer from a Turbulent Boundary Layer on a Porous Sphere," AIAA Paper 76-119, Washington, D.C., Jan. 1976.

[13] Kaattari, G. E., "Effects of Mass Addition on Blunt Body Boundary Layer Transition and Heat Transfer," NASA TP-1139, 1978.

[14] Dorrance, W. H., *Viscous Hypersonic Flow*, McGraw-Hill Book Co., New York, N.Y., 1962, pp. 29-30, 45-56, and 79-88.

[15] Raper, R. M., "Aeroballistic Range Ablation Tests of Candidate Nosetip Materials for the MK500 Reentry Vehicle (U)," Arnold Air Force Station, Tenn., AEDC-TR-75-100, July 1975.

[16] Kratsch, K. M., Loomis, W. C., and Randles, P. W., "Jupiter Probe Heat Shield Design," AIAA Paper 77-427, San Diego, Calif., March 1977.

[17] Wassel, A. T. and Catton, I., "Calculation of Turbulent Boundary Layers over Flat Plates with Different Phenomenological Theories of Turbulence and Variable Turbulent Prandtl Number," *International Journal of Heat and Mass Transfer*, Vol. 16, Aug. 1973, pp. 1547-1563.

[18] Park, C., "Effects of Atomic Oxygen in Graphite Ablation," *AIAA Journal*, Vol. 14, Nov. 1976, pp. 1640-1642.

[19] Park, C., "Stagnation Point Ablation of Carbonaceous Flat Disks in Argon-Filled Ballistic Range, Part 1, Theory," *AIAA Journal*, Vol. 21, Nov. 1983, pp. 1588-1594.

[20] Putz, K. E. and Bartlett, E. P., "Heat-Transfer and Ablation Rate Correlations for Re-entry Heat-Shield and Nosetip Applications," *Journal of Spacecraft and Rockets*, Vol. 10, Jan. 1973, pp. 15-22.

[21] Bartlett, E. P., "Nonsimilar Behavior of Ablating Graphite Sphere Cones," *AIAA Journal*, Vol. 8, May 1970, pp. 948-950.

[22] Lundell, J. H. and Dickey, R. R., "Ablation of Graphitic Materials in the Sublimation Regime," *AIAA Journal*, Vol. 13, Aug. 1975, pp. 1079-1085.

[23] Lundell, J. H. and Dickey, R. R., "Ablation of ATJ Graphite at High Temperatures," *AIAA Journal*, Vol. 11, Feb. 1973, pp. 216-222.

[24] Green, M. J. and Davy, W. C., "Numerical Simulation of Experiments in the Giant Planet Facility," *AIAA Progress in Astronautics and Aeronautics, Entry Heating and Thermal Protection*, Vol. 69, edited by W. G. Olstad, AIAA, New York, 1980.

[25] Miller, J. T., "Aeroballistic Range Tests of Ablating Heat Shield Materials—Interim Report (U)," Arnold Air Force Station, Tenn., AEDC-TR-70-114, May 1970.

[26] Park, C., "Stagnation-Point Ablation of Carbonaceous Flat Disks in Argon-Filled Ballistic Range, Part 2, Experiment," *AIAA Journal*, Vol. 21, Dec. 1983, pp. 1748-1754.